JOURNAL OF ENGINEERING AND TECHNOLOGY, Vol. 9 No. 1 June 2011 ISSN 1684-4114

http://www.iutoic-dhaka.edu/jet

# Numerical Simulation of Axisymmetric Shock Wave Propagation over a Cone

**Mohammad Ali Jinnah***

Received 12 May 2011; Accepted after revision 30 June 2011

## ABSTRACT

***In the present work, a numerical simulation has been conducted for the axisymmetrical shock wave propagation over a cone by solving the Navier-Stokes equations. A two-dimensional domain is taken to solve the axisymmetric problem and a plane shock wave with the Mach number, $M_s$ = 2.38 that propagates from left to right and interacts with a cone surface. The cone apex angle is 86°. Different flow parameters are determined numerically at different positions of the shock wave on the cone to clarify the effects of viscosity and heat conductivity during shock reflection in the conical flow. It is observed that the surface heat flux rate and wall skin friction across the shock are more as compared to other places on cone surface behind the shock wave. The transition point from regular to Mach reflection can hardly be identified if the delayed transition occurs relatively close to the cone apex. The triple point trajectory is drawn for the shock wave propagation over the cone and the transition point is found for the shock wave position of 2.5-3.5 mm from the tip point. The advantages of the numerical simulation are accurate identification of the transition point as well as numerical visualization of the Mach reflection phenomena over the cone surface.***

***Keywords:*** *Shock Reflection, Mach Reflection, Triple Point, Heat Flux, Skin Friction, Conical-flow.*

* *Mechanical and Chemical Engineering Department, Islamic University of Technology (IUT), BoardBazar, Gazipur-1704, Bangladesh. Email: jinnah@iut-dhaka.edu*

## 1 INTRODUCTION

Shock wave propagation over a cone is one of the basic research topics of shock dynamics and in the field of aerodynamics; many researcher conducted experiments on the interaction of shock wave with a body of different geometric shape like wedge, sphere and cylinder etc and they simulated properly with numerical results but due to complex and three dimension phenomena of the shock wave propagation over a cone, few simulation results on shock wave interaction with a cone validated with experimental results. In this field, there have many topics still under research conditions. In the present works, it is tried to calculate some results on axis-symmetric shock wave propagation over a cone numerically and to clarify the process of shock reflection from the cone, the conical flow over the cone and the Mach reflection from the cone surface. Generally such types of interaction effects are seen in aero-mechanism system such as transport aircraft of supersonic and hypersonic speed.

The study of the interaction of shock wave with solid body of different geometric shapes started from various aspects, in them, the shock wave interaction with sphere, cylinder and wedge were important topics. Watanabe and Takayama [1] visualized the reflection of a blast wave from a tilted cone. A planar shock wave of Mach number 1.2 was discharged from the end of a 230 *mm* diameter shock tube into open air and impinged immediately on a cone of apex angle 70$^o$, which was tilted by 25$^o$ from the shock tube axis. Hence, the shock impingement angle on the cone surface varied locally from 45$^o$ to 95$^o$. The resulting shock wave reflection pattern varied from Mach reflection to regular reflection depending on the local intersecting angle. With double exposure holographic interferometry, they observed the reflected shock transition from regular to Mach reflection over the tilted cone. In shock propagation over a convex cylinder, the shock reflection pattern starts as a first regular reflection then changes over to Mach reflection with the decrease in wall inclination angle. Ben-Dor et al. [2] determined the critical transition angles from regular to Mach reflection over a cylinder and from Mach to regular transition over a concave wall for a wide range of shock Mach numbers. The measurement was carried out by using a streak camera in which the feet of shock wave traces on curved walls were visualized through curved slits closely overlaid on these curved walls. In the transition from regular to Mach reflection the onset of Mach stems and slip lines clearly indicated the transition point; in the transition from Mach to regular reflection the disappearance of slip lines distinctly showed the transition point. Takayama and Sasaki [3] later clarified, by using double exposure holographic interferometry, the effect of radii of curvature of these curved walls. They concluded that critical transition angles at given shock Mach number over curved walls varied depending upon radii of curvature. Such results disagreed with those predicted by inviscid analytical models that ignored the existence of wall boundary layers.

Kitade [4] investigated shock wave transitions over a cylinder and revealed that in a series of experiments at identical shock Mach number but with reduced initial pressure (i.e. reduced Reynolds number), the critical angle for the transition from regular to Mach reflection increased. This trend implies that the transition angle decreases to the value predicted by the detachment criterion. These findings clearly indicate that the effect of the Reynolds number on reflected shock transitions should be taken into account. Kosugi [5] and Kitade [4] analyzed numerically the Reynolds number effect on reflected shock transitions over curved walls, and eventually clarified that the Reynolds number affected the critical transition angle over curved walls. Heilig [6] measured the critical transition angles from regular to Mach reflection over a cylinder, compared his measurement with results of the two-shock theory and found that the pressure behind a reflected shock over wedges became a maximum at the critical transition angle. Distributing pressure transducers, he also measured time variation of pressures at various spots over the cylinder surface. However, due to limited spatial resolution of pressure transducers, it was impossible to identify such a distinct increase in pressure values at the transition point. From these time variations of pressure distributions he was able to estimate the unsteady drag on a shock-loaded cylinder.

Mach reflections over cones are common in relation to many practical engineering situations but have received much less attention than have wedge cases. Some experimental work is available for both external and internal conical configurations. In former studies, Bryson and Gross [7], and Takayama and Sekiguchi [8] examined plane shock wave reflection at the external surface of simple, upstream facing cones (i.e apex upstream). More recently, Yang et al. [9] determined the transition angles from regular to Mach reflection and found that, in conical cases, they were close to but somewhat smaller than the wedge values. They also found that the von Neumann reflection range was extended. In the present study, shock wave propagation over a cone is examined numerically by solving two-dimensional Navier-Stokes equations with adaptive grid technique. Here grid adaptation is the improve technique for numerical simulation of the shock wave interaction with a cone.

## 2 NUMERICAL METHODS

### 2.1 Governing equation

In the present computations, the two-dimensional Navier-Stokes equations are solved. Without external forces and heat sources, the conservative form of non-dimensionalized governing equation in two-dimensional Cartesian coordinate system is,

$$\frac{\partial Q}{\partial t}+\frac{\partial (F-Fv)}{\partial x}+\frac{\partial (G-Gv)}{\partial y}=0$$

where, $Q=[\rho, \rho u, \rho v, e]$,

$F=[\rho u, \rho u^2, \rho uv, u(e+p)]$,

$G=[\rho v, \rho uv, \rho v^2, v(e+p)]$,

and $Fv=[0, \tau_{xx}, \tau_{xy}, u\tau_{xx}+v\tau_{xy}-q_x]$

$Gv=[0, \tau_{xy}, \tau_{yy}, u\tau_{xy}+v\tau_{yy}-q_y]$

Here $Q$ is the vector of conservative variables, $F$ and $G$ are inviscid flux vectors, $Fv$ and $Gv$ are viscous flux vectors. Also $\rho$ is the fluid density, $u$ and $v$ are the velocity components in each direction of Cartesian coordinates. While $e$ is the total energy per unit volume, pressure $p$ can expressed by the following state equation for ideal gas,

$$p=(\gamma-1)[e-\tfrac{1}{2}\rho(u^2+v^2)]$$

From the relationship between stress and strain and assumption of stokes, non-dimensional stress components are as follows

$$\tau_{xx}=\frac{\mu}{\mathrm{Re}}\,\tfrac{2}{3}\left(2.\frac{\partial u}{\partial x}-\frac{\partial v}{\partial y}\right),\ \tau_{yy}=\frac{\mu}{\mathrm{Re}}\,\tfrac{2}{3}\left(2.\frac{\partial v}{\partial y}-\frac{\partial u}{\partial x}\right),\ \tau_{xy}=\frac{\mu}{\mathrm{Re}}\left(\frac{\partial v}{\partial x}+\frac{\partial u}{\partial y}\right)$$

The element of heat flux vectors are expressed by Fourior law of heat conduction as

$$q_x=\frac{k}{\mathrm{Re}}\frac{\partial T}{\partial x},\ q_y=\frac{k}{\mathrm{Re}}\frac{\partial T}{\partial y}$$

where $T$ is the temperature and $k$ is the thermal conductivity.

The expression of the thermal conductivity is $k/k_o= c_k\,(T/T_o)^{1.5}$ where $k_o$ is the thermal conductivity at the ambient temperature ($T_o$) and the value of the coefficient, $c_k$ depends on the temperature and the ambient gas.

The expression of viscosity is $\mu/\mu_o= c_v.(T/T_o)^{1.5}$ where $\mu_o$ is the viscosity at the ambient temperature and the coefficient, $c_v$ depends on the temperature and the ambient gas.

The Reynolds number of the flow is defined by $\mathrm{Re}=(\rho_c u_c l_c/\mu_o)$

where $\rho_c$, $u_c$, $l_c$ and $\mu_o$ are respectively a characteristics density, a characteristics velocity, a characteristics length and the viscosity of the fluid.

In the case of Nitrogen, the expression of the thermal conductivity is $k/k_o = c_k (T/T_o)^{1.5}$

where the value of $k$ at $0^oC$ is $0.024\ W/m\text{-}K$ and

The value of the coefficient, $c_k = (1+167/T_o)/(T/T_o+167/T_o)$.

where $k_o$ is the thermal conductivity at the ambient gas temperature $(T_o=293K)$.

The expression of viscosity is $\mu/\mu_o = c_v (T/T_o)^{1.5}$

where the value of $\mu$ at $0^oC$ is $16.5e\text{-}6\ Pa.S$ and $\mu_o$ is the viscosity at the ambient gas temperature and the value of the coefficient, $c_v = (1+107/T_o)/(T/T_o+107/T_o)$.

The expression of surface skin friction is, $C_f = \dfrac{\tau_w}{0.5\rho_s V_s^2}$

Where $\tau_w$ = wall shear stress, $V_s$ = surface velocity

The following characteristics values are used for these computations:

*c_temperature = 293.00 Kelvin*

*c_length = 0.0010 Meter*

*c_pressure = 2000 Pascal*

*Universal Gas constant = 8.314510*

*Moleculer weight, awm = 0.0281*

*Ratio of specific gas constant, gama = 1.4*

*c_velocity = (gas constant*c_temperature/awm)*$^{1/2}$ *= 294.44 m/s*

*c_density = c_pressure/(c_velocity*c_velocity) = 0.0231 kg/m*$^3$

*c_time = c_length/c_velocity = 3.4 μsec*

*c_k =* $k_o$

*c_mu =* $\mu_o$

Pr = *gama /( gama -1.)*c_mu*gas constant/(awm* c_k) = 0.707*

Re = *c_density*c_velocity*c_length/c_mu = 387*

## 2.2 Spatial discretization

The governing equation described above for the compressible viscous flow is discretised by the finite volume method. A second order, upwind Godounov scheme of Flux vector splitting method is used to discrete the inviscid flux terms and MUSCL-Hancock scheme is used for interpolation of variables where HLLC Reimann solver is used for shock capturing in the flow. Central differencing scheme is used in discretizing the viscous flux terms. The control volume is taken to be a ring-shaped volume with a quadrilateral cross-section, which naturally removes the source terms in the mass and energy equations.

## 2.3 Grid Systems and Grid Adaptation

Two-dimensional quadrilateral cells with adaptive grid systems are used in these computations. In this grid systems, the cell-edge data structures are arranged in such a way that each cell contains four faces which are sequence in one to four and each face indicates two neighboring cell that is left cell and right cell providing all faces of a cell are vectorized by position and coordinate in the grid systems. The initial number of cell is 2240 and the total area of the two-dimensional domain is 914 $mm^2$ which are shown in **Fig.1**. So the average area of the coarse grid without refinement is 0.41 $mm^2$.

The grid adaptation is one of the improved and computational time saving techniques, which is used in these computations. The grid adaptation is performed by two procedures one is refinement procedure and another is coarsening procedure. The refinement and coarsening operations are handled separately in computation. The criterion used for grid adaptation is based on the truncation error ($\epsilon_T$) of the Taylor series expansion of density. In these computations, the value of $\alpha_f$ is used 0.02 and it is problem-independent parameter. The refinement and coarsening operation for any cell depends on $\epsilon_T$

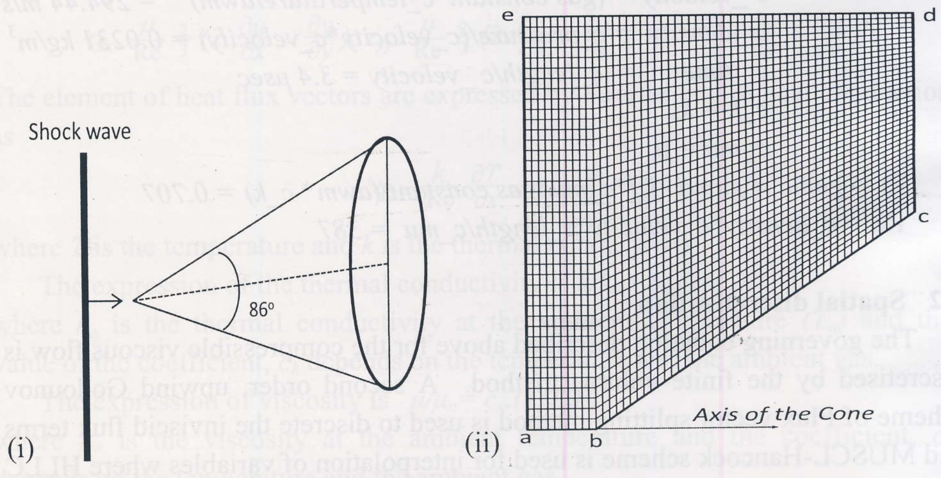


**Figure 1:** (i) Three-dimensional cone where the shock wave propagation direction is shown, (ii) Two- dimensional numerical grids for axis-symmetric domain *abcde* where the axis of the cone passes through line *ab*.

value and this $\epsilon_T$ value is determined for each face of a cell. The criterion for adaptation for any cell is,

Refinement = maximum $\epsilon_T$ of four faces of a cell > $\varepsilon_r$

Coarsening = maximum $\epsilon_T$ of four faces of a cell < $\varepsilon_c$

where $\varepsilon_r$ and $\varepsilon_c$ are the threshold values for refinement and coarsening. In the computations, the values of $\varepsilon_r$ are used 0.30~0.34 and the values of $\varepsilon_c$ are used 0.26~0.30 and the level of refinement is 6.

In the refinement procedure, the cells are selected for refinement in which every cell is divided into four new sub cells and these new sub cells are arranged in a particular sequence so that these sub cells are used suitably in the data-structure. In the coarsening procedure, the four sub cells, which are generated from the primary cell, are restored into primary cell.

### 2.4 Boundary conditions

The two-dimensional domain *abcde*, shown in **Fig.1**, is used in these computations where the line *ab* is taken as an axis-symmetric boundary line. The line, *ae* is an inflow boundary line and the cone surface, *bc* is taken as solid boundary. The upstream of incident shock wave is set as an inflow boundary condition, the properties and velocities of which are calculated from Rankine-Hugoniot conditions with incident Mach number. The downstream inflow boundary condition and the wall surface are used as solid boundary conditions where the gradients normal to the surface are taken zero. All solid walls are treated as viscous solid wall boundary. The initial temperature of the solid wall is constant and is equal to ambient temperature. No external heat crosses the solid boundary. For the axis-symmetric boundary, all fluxes, cross the boundary, are taken to zero.

## 3 RESULTS AND DISCUSSION

In the present numerical simulation, the axisymmetric shock wave propagation over a cone has been studied by solving two-dimensional Navier-Stokes equations with adaptive grid technique. A plane shock wave with the Mach number, $M_s$=2.38, propagates from left to right and reflects from the cone surface in Nitrogen. The cone apex angle is 86$^o$ which is shown in **Fig.1.** Despite solving the identical initial and boundary conditions, many researchers got several numerical results where there had some variations with each other and also getting some experimental results were quite very difficult due to three dimensional interaction effects. So the present problem is still under research conditions. The present numerical studies are trying to explain on some aspects of shock wave interaction with the cone. The shock reflection phenomena from the cone surface, the skin friction and the surface heat flux due to shock wave propagation over the cone are the major observations.

Two basic types of shock wave reflection configurations are known to take place. Regarding two-dimensional shock wave reflections, their patterns are classified, in general, as regular reflection or Mach reflection, depending on shock wave Mach numbers, cone angles, and ratios of specific heats of test gases. Regular Reflection (RR) takes place from the tip of the cone. Mach Reflection (MR) occurs for the surface inclinations. However, regular and Mach reflections can coexist, in particular, over a three-dimensional cone surface, whose inclination angles locally vary normal to the direction of shock propagation. The change-over criteria from RR to MR (and vice versa) has been the subject of numerous investigations over the past 65 years. Von Neumann [10] found that with regards to transition, the phenomenon needed to be subdivided into a weak and a strong reflection domain. The weak domain presents an interesting and highly challenging impasse for the onset of weak MR. In the range of RR, the reflected shock wave behaves and agrees quite accurately with the theory of Rankine-Hugoniot (RH). While the most comprehensive analysis of the two main shocks reflection configurations has been provided by von Neumann [10], a diagram of RR which covers the entire range of physically meaningful shock strengths (from the acoustic limit up to infinitely strong incident shock waves and based on ideal gas behaviour) may be found in Courant and Friedrichs ([11]). Normally at the terminating point of RR, the reflected shock has reached its maximum flow deflecting capacity. In the reflection patterns over the surface of a simple cone, all figures in **Fig.2** show identical and demonstrate that self-similarity does exit.

In shock propagation over a cone, the shock reflection pattern starts as a first regular reflection then changes over to Mach reflection with the increase in cone surface inclination angle. The Mach reflection consists of the Mach stem and the incident shock wave as well as the shock front. By using the density contour for shock propagation, the Regular Reflection (RR) and after certain period, the Mach Reflection (MR) are described properly which are shown in **Fig.2** (i), (ii), (iii) and (iv) at different positions of the shock wave over the cone. It is shown in **Fig.2** that for the different shock positions at *05, 10, 15* and *20 mm* from the tip of the cone, the shock wave travelling time over the cone are 60.4 *μsec*, 120.8 *μsec,* 181.2 *μsec* and 241.6 *μsec* respectively. The present analysis

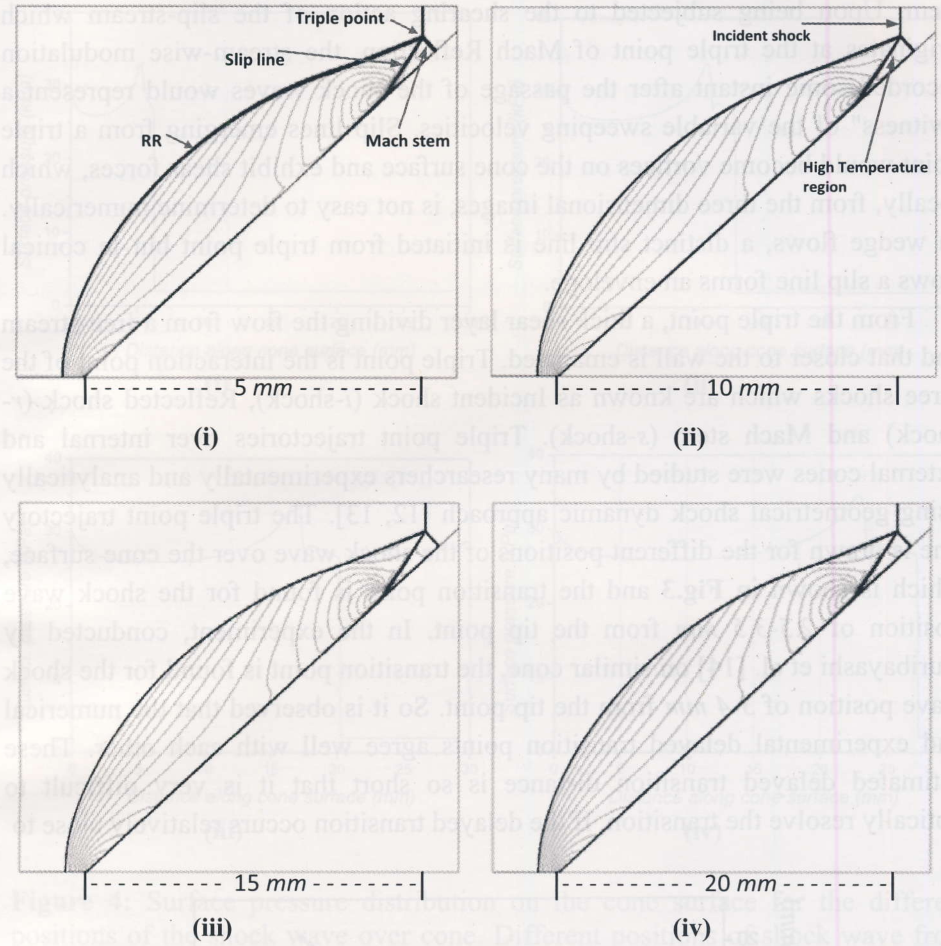


shows that the triple point position is determined by the pressure wave arising from the initial impact of the incident shock at the tip of the cone, modified by pressures propagating from the surface along the Mach stem. It is observed that the region between the Mach stem and the slipstream shows only minor density gradients and the small density contour near the base of the Mach stem may be due to the rapid change in the local shock direction from the triple-point to the wall surface.

The analysis used to obtain the triple point path also gives a local value for the tangent of the reflected wave at the triple point and a speed for the cylindrical wave propagating from the tip impact. Behind the triple point where the three shocks meet, a slip line marks the discontinuity in entropy between the gas that went through the incident and reflected shocks and the gas that crossed the Mach stem. Upon being subjected to the shearing action of the slip-stream which originates at the triple point of Mach Reflection, the stream-wise modulation recorded some instant after the passage of the shock waves would represent a "witness" of the variable sweeping velocities. Slip lines emerging from a triple point would become vortices on the cone surface and exhibit shear forces, which locally, from the three dimensional images, is not easy to determine numerically. In wedge flows, a distinct slip line is initiated from triple point but in conical flows a slip line forms an envelope.

From the triple point, a thick shear layer dividing the flow from a free-stream and that closer to the wall is emanated. Triple point is the interaction point of the three shocks which are known as Incident shock (*i*-shock), Reflected shock (*r*-shock) and Mach stem (*s*-shock). Triple point trajectories over internal and external cones were studied by many researchers experimentally and analytically using geometrical shock dynamic approach [12, 13]. The triple point trajectory line is drawn for the different positions of the shock wave over the cone surface, which is shown in **Fig.3** and the transition point is found for the shock wave position of *2.5-3.5 mm* from the tip point. In the experiment, conducted by Kuribayashi et al. [14] on similar cone, the transition point is found for the shock wave position of *3-4 mm* from the tip point. So it is observed that the numerical and experimental delayed transition points agree well with each other. These estimated delayed transition distance is so short that it is very difficult to optically resolve the transition. If the delayed transition occurs relatively close to

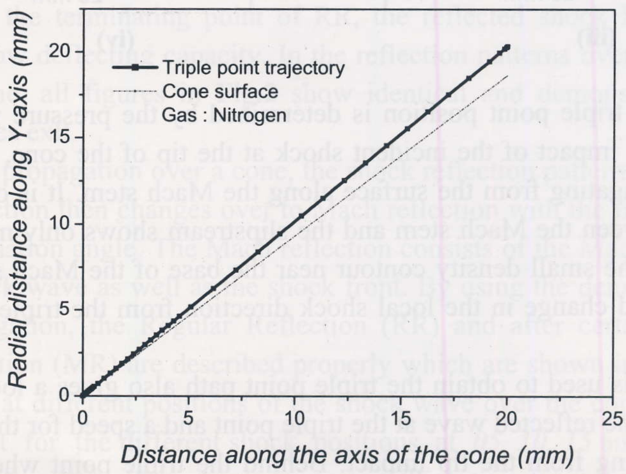


**Figure 3:** Triple point trajectory line for the different position of the shock wave from the tip of the cone.

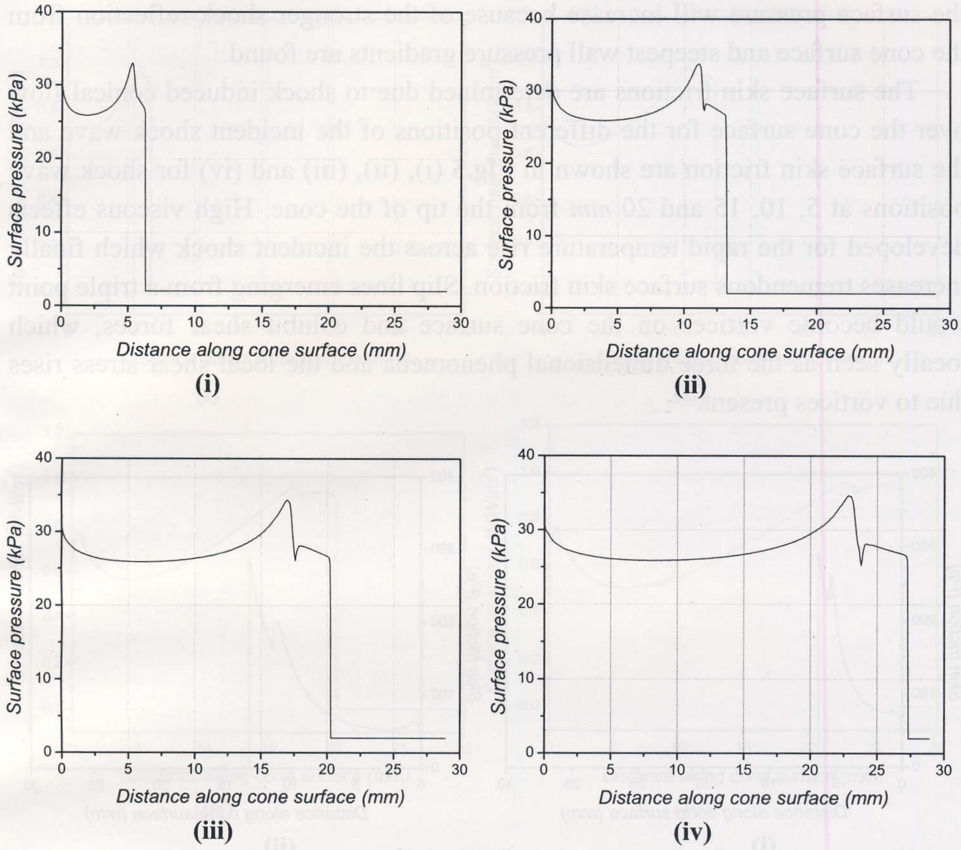


**Figure 4:** Surface pressure distribution on the cone surface for the different positions of the shock wave over cone. Different positions of shock wave from the tip of the cone are; (i) *05mm*, (ii) *10mm*, (iii) *15mm* and (iv) *20mm*.

the cone apex, we can hardly identify the transition point from regular to Mach reflection from numerical visualization images, unless the spatial resolution is too good. In wedge cases, the delayed transition distance becomes longer for smaller *Re* because the boundary layer displacement thickness becomes thicker by reducing the initial pressure.

The surface pressures of the cone are determined numerically for different shock positions which are shown in **Fig.4** (i), (ii), (iii) and (iv). Due to higher shear stress developed during shock wave propagation over conical surface, surface pressures rise behind the normal Mach stem and the pressure decreases as the far distance behind the incident shock wave. Normally the surface pressure variations depend on the apex angle of the cone. As increasing the apex angle, the surface pressure will increase because of the stronger shock reflection from the cone surface and steepest wall pressure gradients are found.

The surface skin frictions are determined due to shock induced conical flow over the cone surface for the different positions of the incident shock wave and the surface skin friction are shown in **Fig.5** (i), (ii), (iii) and (iv) for shock wave positions at 5, 10, 15 and 20 *mm* from the tip of the cone. High viscous effects developed for the rapid temperature rise across the incident shock which finally increases tremendous surface skin friction. Slip lines emerging from a triple point would become vortices on the cone surface and exhibit shear forces, which locally seen as the three dimensional phenomena and the local shear stress rises due to vortices present.

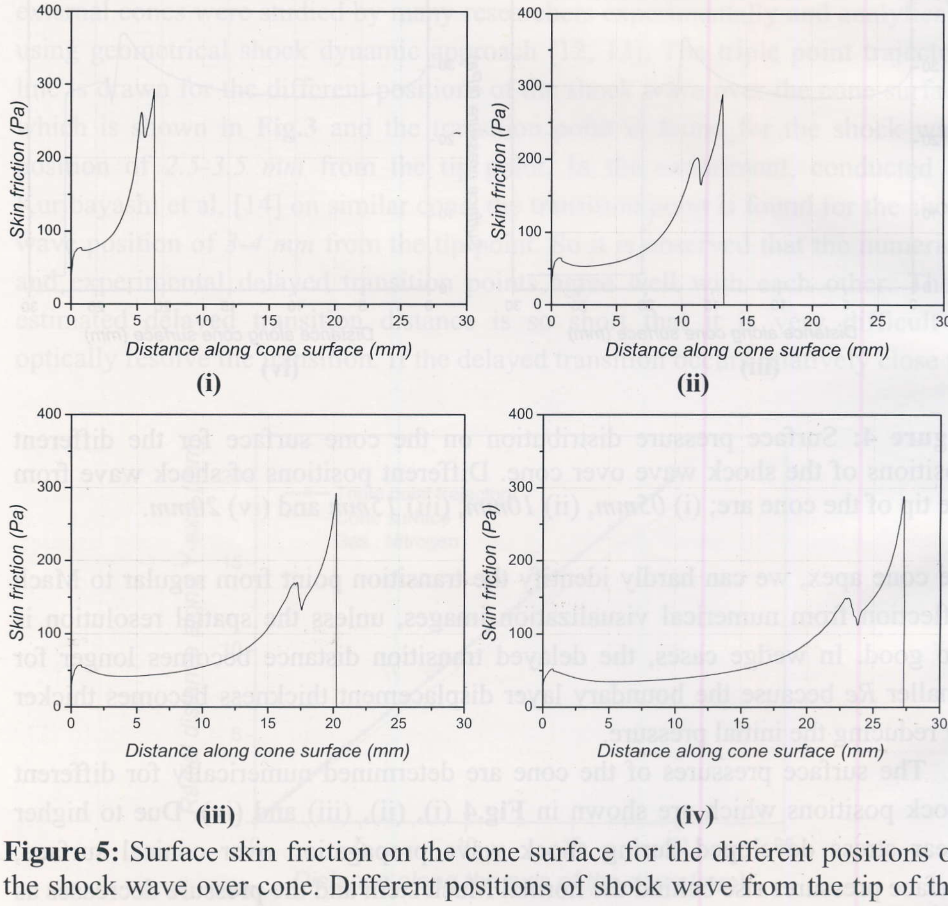


**Figure 5:** Surface skin friction on the cone surface for the different positions of the shock wave over cone. Different positions of shock wave from the tip of the cone are; (i) *05mm*, (ii) *10mm*, (iii) *15mm* and (iv) *20mm*.

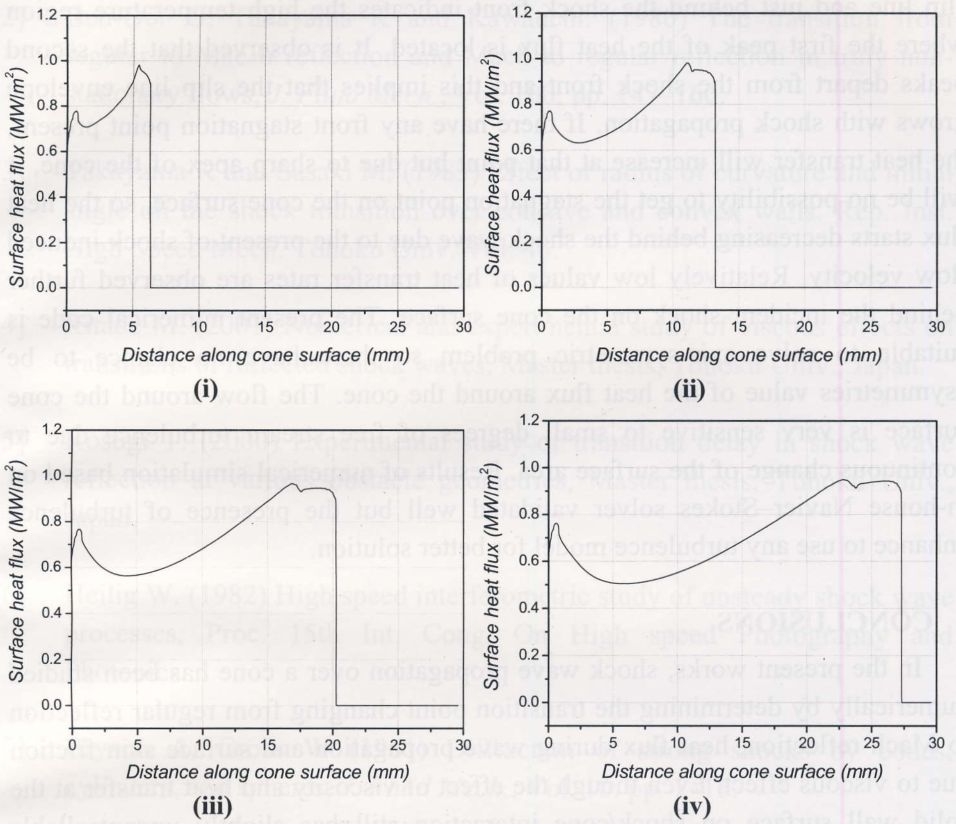


**Figure 6:** Surface heat flux on the cone surface for the different positions of the shock wave over cone. Different positions of shock wave from the tip of the cone are; (i) *05mm*, (ii) *10mm*, (iii) *15mm* and (iv) *20mm*.

**Fig.6** (i), (ii), (iii) and (iv) summarize heat flux distributions when the incident shock wave arrived at 5, 10, 15, and 20 *mm* from the apex of the cone. Abscissa shows the distance along the cone surface from the apex in *mm* and ordinate heat flux in $MW/m^2$. The resolution of heat flux on the cone surface is strongly governed by the grid size and the ratio of quadrilateral grid geometry. For the smaller grid size around 6.5 micron, the first peak of heat flux will be so sharp and such type of solutions are so difficult by the normal computer and it is quite impossible to measure this peak by the laboratory experiment. In many places of the present heat flux variations are agreed with the experimental results conducted by Kuribayashi et al. [14]. It is seen in **Fig.6** that a second peak of heat flux appears just behind the first peak of heat flux in the numerical results which indicates the presence of the slip line envelop and the region between the slip line and just behind the shock front indicates the high temperature region where the first peak of the heat flux is located. It is observed that the second peaks depart from the shock front and this implies that the slip line envelope grows with shock propagation. If there have any front stagnation point present, the heat transfer will increase at that point but due to sharp apex of the cone, it will be no possibility to get the stagnation point on the cone surface, so the heat flux starts decreasing behind the shock wave due to the present of shock induced flow velocity. Relatively low values of heat transfer rates are observed further behind the incident shock on the cone surface. The present numerical code is suitable to solve axis-symmetric problem so there have no chance to be asymmetries value of the heat flux around the cone. The flow around the cone surface is very sensitive to small degrees of free stream turbulence due to continuous change of the surface area. Results of numerical simulation based on in-house Navier–Stokes solver validated well but the presence of turbulence enhance to use any turbulence model for better solution.

## 4 CONCLUSIONS

In the present works, shock wave propagation over a cone has been studied numerically by determining the transition point changing from regular reflection to Mach reflection, heat flux during wave propagation and surface skin friction due to viscous effect. Even though the effect of viscosity and heat transfer at the solid wall surface on shock/cone interaction still has slightly uncontrollable factors in CFD but the present simulation works are providing better solutions where grid adaptation technique is used. The grid adaptation can also give the results which ultimately independent of the grid size. Gradually the flow fields may change due to increasing the cone surface area as well as increasing the surface frictions and heat fluxes with increasing the three dimensional effects in the flow fields. The presence of turbulent boundary on the cone surface indicates the turbulence present in the conical flow due to tremendous viscous effects near the slip line.

## REFERENCES

[1] Watanabe M and Takayama K. (1993) Study of reflected shock wave transition over a cone with an angle of attack. In: 1993 Japanese Shock Wave Symp. Sendai, pp. 689–692.This paper is available in ISWI Proceedings Archive 2007, which contains Japanese Shock Wave Symposium since 1989 offered by ITOCHU Techno-Solutions.

[2] Ben-Dor G, Takayama K and Kawauchi. (1980) The transition from regular to Mac h reflection and Mach to regular reflection in truly non-stationary flows, *J. Fluid Mech.*, Vol. 100: pp. 147–160.

[3] Takayama K and Sasaki M. (1983) Effect of radius of curvature and initial angle on the shock transition over concave and convex walls. Rep. Inst. High Speed Mech. Tohoku Univ. Vol. 46.

[4] Kitade M. (2001) Numerical and experimental study of viscous effects on transitions of reflected shock waves, Master thesis, Tohoku Univ., Japan.

[5] Kosugi T. (2000) Experimental study of transition delay in shock wave reflection at various obstacle geometries, Master thesis, Tohoku Univ., Japan.

[6] Heilig W. (1982) High speed interferometric study of unsteady shock wave processes, Proc. 15th Int. Cong. On High speed Photography and Photonics.

[7] Bryson A, Gross W (1961) Diffraction of strong shocks by cones, cylinders, and spheres, *J. Fluid Mech.*, Vol. 10: pp. 1–16.

[8] Takayama K and Sekiguchi H. (1976) Shock wave reflection by cones. Rept Inst High Speed Mech, Tohoku Univ, Japan Vol. 34: pp. 53–74.

[9] Yang J, Suzuki M and Takayama K. (1995) An investigation of shock wave reflection over cones. In: Proc Japanese Shock Wave Symp, Yokohama, March: pp. 625–628.

[10] Von Neumann J. (1943) Oblique reflection of shocks. See *'John von Neumann - Collected Works',* Vol. 6: pp. 238-299. Pergamon Press, Oxford, 1963.

[11] Courant R and Friedrichs KO. *Supersonic Flow and Shock Waves.* Interscience Publishers, New York, 1948 (also Springer Verlag). *Sciences,* 275 (Série A), 17 Juillet 1972, 225-228.

[12] Han AY, Milton BE and Takayama K. (1992) The Mach reflection triple point locus for internal and external diffraction of a moving shock wave. *Shock Waves*, Vol. 2: pp. 5–12.

[13] Milton B and Archer RD. (1993) Generalized concepts for the internal and external conical Mach reflection of moving shockwaves. In: Brun, R., Dumitrescu, L.Z. (eds.) Proceedings of 19th ISSW Marseille, pp. 157–162.

[14] Kuribayashi T, Ohtani K, Takayama K, Menezes V, Sun M and Saito T. (2007) Heat flux measurement over a cone in a shock tube flow. *Shock Waves*, Vol. 16: pp. 275–285.